

Venc Design and Velocity Estimation for Phase Contrast MRI

Shen Zhao, Rizwan Ahmad, and Lee C. Potter, *Senior Member, IEEE*

Abstract—In phase-contrast magnetic resonance imaging (PC-MRI), the velocity of spins at a voxel is encoded in the image phase. The strength of the velocity encoding (venc) gradient offers a trade-off between the velocity-to-noise ratio (VNR) and the extent of phase aliasing. In the three-point encoding employed in traditional dual-venc acquisition, two velocity-encoded acquisitions are acquired along with a third velocity-compensated measurement; their phase differences result in an unaliased high-venc measurement used to unwrap the less noisy low-venc measurement. Alternatively, the velocity may be more accurately estimated by jointly processing all three potentially wrapped phase differences. We present a fast, grid-free approximate maximum likelihood estimator, *Phase Recovery from Multiple Wrapped Measurements (PRoM)*, for solving a noisy set of congruence equations with correlated noise. PRoM is applied to three-point acquisition for estimating velocity. The proposed approach can significantly expand the range of correctly unwrapped velocities compared to the traditional dual-venc method, while also providing improvement in velocity-to-noise ratio. Moreover, its closed-form expressions for the probability distribution of the estimated velocity enable the optimized design of acquisition.

Index Terms—Phase-contrast imaging; dual venc; phase unwrapping; congruence equations; sparse array design

I. INTRODUCTION

PHASE contrast magnetic resonance imaging (PC-MRI) is a quantitative, non-invasive technique to measure hemodynamics in vivo. Velocity encoding is achieved via a time-varying magnetic field gradient, resulting in a per voxel phase that is proportional to the velocity of spins. Combining PC-MRI with cine imaging allows capturing the hemodynamics through the cardiac cycle [1]. Lowering the first moment of the velocity encoding gradient extends the unaliased range but leads to a lower velocity-to-noise ratio (VNR). To address this issue, dual-venc techniques have been proposed, where VNR is determined by the wrapped, low-venc measurement, and the unwrapping is guided by the high-venc measurement [2], [3]. In contrast, multiple low-venc (and potentially wrapped) measurements may be jointly unwrapped [4], [5], leading to a larger unambiguous range of velocities and reduced estimation

This manuscript was submitted on September 10, 2021. This work was supported in part by NIH grants R01HL135489 and R21EB022277.

S. Zhao and L. Potter are with the Department of Electrical & Computer Engineering, Ohio State University, Columbus, OH 43210 USA (email: zhao.1758@osu.edu, potter.36@osu.edu).

R. Ahmad is with the Department of Biomedical Engineering, Ohio State University, Columbus, OH 43210 USA (email: ahmad.46@osu.edu).

error variance. Such methods, however, perform a computationally expensive grid search to estimate the unaliased velocity and do not guide the selection of optimal venc values.

Building on our preliminary work [4], this paper presents an estimator, *Phase Recovery from Multiple Wrapped Measurements (PRoM)*, for approximate maximum likelihood estimation (MLE) of the encoded velocity component from multiple wrapped measurements with correlated noise. The estimator is used in PC-MRI to jointly process all phase differences in a multi-point encoded acquisition. The PRoM estimator first constructs a small list of candidate wrapping integers; the probability that the true wrapping lies in the set is arbitrarily close to 1. For each candidate, the corresponding velocity estimate is a simple weighted combination of the noisy measurements plus the candidate wrapping, and thus is computed without a grid of quantized velocities. Among the candidate velocities, the estimate is chosen to maximize the likelihood function.

Expressions are derived for root mean squared estimation error and probability of unwrapping errors. These expressions then allow for the optimized design of a three-point acquisition. Additionally, the same estimation problem appears in other array processing applications, where PRoM extends current art [6], [7] to provide: a fast, grid-free estimator; accommodation of correlated noise; and, principled design of sparse array geometry. For validation, we have applied PRoM to simulated three-point encoding data as well measured datasets from a spinning phantom and a healthy volunteer.

II. THEORY

A. Phase Encoding

A time-varying field gradient may be used to encode spin velocity into image phase. Here, we consider encoding a velocity component in one direction. Let γ be the gyromagnetic ratio, B_0 the static magnetic field strength, $g(t)$ the time-varying field gradient, and $p(t)$ the spin position. Consider the Larmor precession frequency, ω , for a spin moving through a magnetic field,

$$\omega(r, t) = \gamma B_0 + \gamma g(t)p(t). \quad (1)$$

The Taylor series expansion of position yields

$$p(t) = r(0) + \frac{v}{1!}t + \frac{a}{2!}t^2 + \dots \quad (2)$$

Thus, to first order $\omega(r, t) \approx \gamma B_0 + \gamma g(t)(p(0) + vt)$. The phase is the integral of the frequency, yielding [8]

$$\phi = \underbrace{\gamma B_0 T_E}_{\phi_0} + \underbrace{\gamma r(0) \int_0^{T_E} g(t) dt}_{m_0} + \underbrace{\gamma v \int_0^{T_E} t g(t) dt}_{m_1}, \quad (3)$$

where m_0 and m_1 are the zeroth and first moments of the gradient waveform, $g(t)$, and T_E is the echo time. So, for $m_0 = 0$, the phase is the scaled velocity plus a background phase, ϕ_0 . The scaling factor γm_1 relates v to $\phi - \phi_0$. Observe that v is unaliased to the range $[-\frac{\pi}{\gamma m_1}, \frac{\pi}{\gamma m_1}]$. For $m_1 = 0$, ϕ is unaffected by v .

For L encodings with first moments m_{1l} , we have the following complex-valued measurements at each spatial location

$$\tilde{y}_l = A_l e^{i(\phi_0 + \gamma m_{1l} v)} + n_l, \quad l = 1, \dots, L, \quad (4)$$

where n_l is i.i.d. complex Gaussian noise with variance $\sigma^2(n_l)/2$ in each of the uncorrelated real and imaginary parts. The noiseless solution is unambiguous on any interval of length $2 \text{LCM}(\frac{\pi}{\gamma m_{11}}, \frac{\pi}{\gamma m_{12}}, \dots, \frac{\pi}{\gamma m_{1L}})$, where LCM denotes least common multiple. Variation of velocity within a voxel causes dephasing, leading to reduction in the measured signal amplitude, A_l . In noise, a smaller $|m_{1l}|$ keeps the signal loss, and hence the phase disturbance, smaller.

The maximum likelihood estimation of v from $\tilde{\mathbf{y}} = [\tilde{y}_1, \dots, \tilde{y}_L]$ is a nonlinear least-squares optimization with a difficult cost surface exhibiting many local minima [9, pp. 179-185]. An example of sum of squared fit error versus velocity using a three-point acquisition is shown in Fig. 1 for $m_{11} = 0$, $\frac{\pi}{\gamma m_{12}} = 50$, and $\frac{\pi}{\gamma m_{13}} = 70$; amplitudes are assumed common, $A_1 = A_2 = A_3$, and the noise is set to make $\frac{A_l}{\sigma(n_l)} = 5$. The error at the true velocity, $v = 0$, is shown by the red diamond, and the global minimum at $v \approx 1.04$ for the given noise realization is shown by the green marker. Competing local minima, shown as blue markers, may become the global minimum due to noise, thereby causing unwrapping errors.

B. Linear Unbiased Estimator

Consider simplification of the data processing by working from the phase differences of the encoded voxels, rather than from the complex-valued voxels directly. We will numerically illustrate in subsection III.A that this simplification has no tangible impact on velocity estimation. For any pair of encodings, the noisy phase differences for $a, b \in (1, \dots, L)$ are given by

$$\tilde{\theta}_{ab} = \angle(\tilde{y}_a \tilde{y}_b^*), \quad a > b, \quad (5)$$

where $\angle(\cdot)$ denotes angle of a complex-valued number, and $(\cdot)^*$ denotes conjugation. We have $\frac{L(L-1)}{2}$ such combinations. The venc resulting from the combinations of conjugate products are

$$\text{venc}_{ab} = \frac{\pi}{\gamma(m_{1a} - m_{1b})}, \quad a > b. \quad (6)$$

Multiplying the venc s with phases, we obtain (possibly wrapped) noisy velocity \tilde{r}_{ab}

$$\tilde{r}_{ab} = \frac{\tilde{\theta}_{ab}}{\pi} \text{venc}_{ab}. \quad (7)$$

Phases $\tilde{\theta}_{ab}$ are unambiguous on an interval of length 2π , and for convenience we use $[0, 2\pi)$. Thus, we have the set of noisy congruence equations in the unknown, v :

$$\tilde{r}_{ab} \equiv (v + n_{ab}) \pmod{2\text{venc}_{ab}}, \quad (8)$$

where n_{ab} is the noise. So, the solution for v is unambiguous on any interval of length Ω ,

$$\Omega = 2 \text{LCM}(\{\text{venc}_{ab} | a > b\}). \quad (9)$$

We use the range $[0, \Omega)$ for convenience, and note that there is a one-to-one association between $v \in [0, \Omega)$ and $v \in [-\Omega/2, \Omega/2)$ under periodicity. Define a vector, \mathbf{k} , of $\frac{L(L-1)}{2}$ wrapping integers. Momentarily assume true wrapping integers, \mathbf{k} , are known. For L velocity encoded measurements, we can rewrite (8) as a linear least squares problem:

$$\tilde{\mathbf{r}} + 2\mathbf{k} \circ \mathbf{venc} = v\mathbf{1} + \mathbf{n}, \quad (10)$$

where \circ is the Hadamard (element-wise) product and

$$\begin{aligned} \tilde{\mathbf{r}} &= [\tilde{r}_{21}, \dots, \tilde{r}_{L(L-1)}]^\top \\ \mathbf{venc} &= [\text{venc}_{21}, \dots, \text{venc}_{L(L-1)}]^\top \\ \mathbf{k} &= [\mathbf{k}_{21}, \dots, \mathbf{k}_{L(L-1)}]^\top \\ \mathbf{1} &= [1, \dots, 1]^\top \\ \mathbf{n} &= [n_{21}, \dots, n_{L(L-1)}]^\top. \end{aligned}$$

To obtain \hat{v} , the linear unbiased estimator of v , from $\tilde{\mathbf{r}}$ with smallest root mean squared error, we need only the covariance matrix of the noise in the remainders, $\Sigma(\mathbf{n})$. To proceed, we assume noiseless amplitudes are equal, $A_l = A$, and assume equal noise power, $\sigma(n_l) = \sigma$. Define signal to noise ratio on the complex-valued voxel, $\text{snr} = \frac{A}{\sigma}$. Our first approximation is that \mathbf{n} follows a joint Gaussian distribution. Then, starting

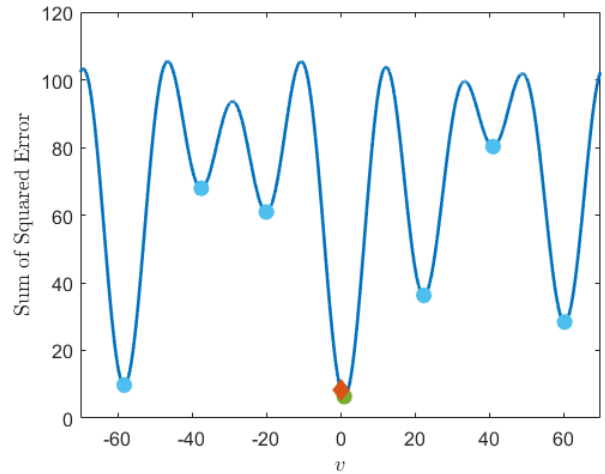


Fig. 1. Example sum of squared error versus velocity for a three-point encoding. The error at the true velocity $v = 0$ is shown by the red diamond. The global minimum at $v \approx 1.04$ for the given noise realization is shown by the green marker. Competing local minima, shown as light blue markers, may become the global minimum due to noise, thereby causing unwrapping errors.

with the product $y_a y_b^*$, we can obtain the covariance matrix

$$\sigma^2(n_{ab}) = \frac{(1 + 2\text{snr}^2)\text{venc}_{ab}^2}{2\pi^2\text{snr}^4}, \quad (11)$$

$$\text{cov}(n_{ab}, n_{cb}) = \frac{\text{venc}_{ab}\text{venc}_{cb}}{2\pi^2\text{snr}^2}. \quad (12)$$

Note $\text{cov}(n_{ab}, n_{cd}) = 0$ for $(a, b) \cap (c, d) = \emptyset$ (that is, when phase differences are computed without a shared measurement). See Appendix I both for derivation of (11), (23) and for extension to the more general case of unequal noiseless amplitudes, A_l , due to dephasing. Given the true wrapping integers \mathbf{k} , the linear minimum mean squared error estimator $\hat{v}_{\mathbf{k}}$ and resulting RMSE, $\sigma(\hat{v}_{\mathbf{k}})$, are

$$\hat{v}_{\mathbf{k}} = \langle \mathbf{w}^\top (\tilde{\mathbf{r}} + 2\mathbf{k} \circ \mathbf{venc}) \rangle_\Omega \quad (13)$$

$$\mathbf{w}^\top = \frac{\mathbf{1}^\top \Sigma^{-1}(\mathbf{n})}{\mathbf{1}^\top \Sigma^{-1}(\mathbf{n}) \mathbf{1}} \quad (14)$$

$$\sigma(\hat{v}_{\mathbf{k}}) = \mathbf{w}^\top \Sigma(\mathbf{n}) \mathbf{w}, \quad (15)$$

where $\langle \cdot \rangle_\Omega$ is remainder of a real number modulo Ω . Thus, the $\hat{v}_{\mathbf{k}}$ is a weighted sum of unwrapped noisy velocities. The second approximation we adopt is

$$\mathbb{P}(-\mathbf{venc} \preceq \mathbf{n} \preceq \mathbf{venc}) \approx 1, \quad (16)$$

where \preceq is element-wise less than or equal. The likelihood $\mathbb{P}(\tilde{\mathbf{r}}|v)$ then can be approximated as

$$\mathbb{P}(\tilde{\mathbf{r}}|v) \approx \frac{e^{-\frac{1}{2}d_{2\text{venc}}^\top(\tilde{\mathbf{r}}, v\mathbf{1})\Sigma^{-1}(\mathbf{n})d_{2\text{venc}}(\tilde{\mathbf{r}}, v\mathbf{1})}}{\det(2\pi\Sigma^{-1}(\mathbf{n}))} \quad (17)$$

$$d_z(\mathbf{x}, \mathbf{y}) \triangleq \mathbf{x} - \mathbf{y} - \text{round}\left(\frac{\mathbf{x} - \mathbf{y}}{z}\right) \circ z, \quad (18)$$

where $d_z(\mathbf{x}, \mathbf{y})$ is a ‘‘wrapped distance’’ between \mathbf{x} and \mathbf{y} modulo z . One could perform search over all possible \mathbf{k} to minimize the negative log likelihood,

$$\mathcal{L}(\tilde{\mathbf{r}}, \hat{v}_{\mathbf{k}}) = \frac{1}{2}d_{2\text{venc}}^\top(\tilde{\mathbf{r}}, \hat{v}_{\mathbf{k}}\mathbf{1})\Sigma^{-1}(\mathbf{n})d_{2\text{venc}}(\tilde{\mathbf{r}}, \hat{v}_{\mathbf{k}}\mathbf{1}). \quad (19)$$

In subsection II-E, we instead present a fast method to detect the best wrapping integers, \mathbf{k}^* .

In the subsections II-C and II-G, we explicitly consider three-point encoding, $L = 3$, to provide concrete results and to optimize the design of \mathbf{venc} and underlying first moments $[m_{11}, m_{12}, m_{13}]$.

C. Three-point Encoding

We consider here three-point encoding for velocity in one direction. Notice from (6) and (9) that every venc_{ab} , and hence the unambiguous range, Ω , depend only on the differences between first moments; thus, venc_{ab} and Ω are unaffected by adding the same constant to every first moment. We assume the following ordering for the first moments:

$$m_{11} < m_{12} < m_{13}, m_{12} - m_{11} < m_{13} - m_{11}. \quad (20)$$

For convenience, we list the three vencs from (6) in ascending order with indices 1, 2, 3, and correspondingly order $\boldsymbol{\theta}$, $\tilde{\mathbf{r}}$, \mathbf{k} , and \mathbf{n} :

$$\mathbf{venc} = [\text{venc}_{31}, \text{venc}_{32}, \text{venc}_{21}]^\top. \quad (21)$$

Let $R = \frac{\text{venc}_{32}}{\text{venc}_{31}}$, noting that (6) and (20) imply $R \in (1, 2)$. For rational $R = p/q$ with co-prime integers p and q , the unambiguous range Ω in (9) is

$$\Omega = 2(p - q)\text{venc}_{21}. \quad (22)$$

Thus, by jointly unwrapping multiple vencs one can construct an unaliased velocity range much larger than the highest venc_{21} .

From (11) and (23), the 3-by-3 covariance matrix is

$$\Sigma(\mathbf{n}) = \frac{\text{venc}_{31}^2}{2\pi^2\text{snr}^4} \begin{bmatrix} 1 + 2\text{snr}^2 & \text{snr}^2 R & \frac{\text{snr}^2 R}{R-1} \\ \text{snr}^2 R & (1 + 2\text{snr}^2)R^2 & \frac{-\text{snr}^2 R}{R-1} \\ \frac{\text{snr}^2 R}{R-1} & \frac{-\text{snr}^2 R^2}{R-1} & \frac{(1+2\text{snr}^2)R^2}{(R-1)^2} \end{bmatrix}. \quad (23)$$

The expression in (14) admits closed-form solution in terms of the encodings only and independent of the snr:

$$\mathbf{w}^\top = \frac{1}{2(R^2 - R + 1)} [R^2 \quad 1 \quad (-1 + R)^2]. \quad (24)$$

Further, for random noise \mathbf{n} , the resulting standard deviation given wrapping integers \mathbf{k} , is

$$\sigma(\hat{v}_{\mathbf{k}}) = \text{venc}_{31} \sqrt{\frac{(1 + 3\text{snr}^2)}{2\pi^2\text{snr}^4}} \sqrt{\frac{R^2}{2(R^2 - R + 1)}}. \quad (25)$$

Analogous expressions for minimum variance estimation in the presence of unequal magnitudes A_l are given in Appendix I. The three terms in (25) from left to right specify the dependence of the velocity estimation error on, respectively: the smallest venc , the voxel SNR, and ratio of vencs. Armed with the explicit error variance in (25) and the probability of unwrapping errors derived below, we present in Section II-G an optimized design of \mathbf{venc} for three-point encoding, given a desired unambiguous range of velocities to be observed and snr.

D. Existing Dual Venc Estimators

In the notation of (7) and (21), the approaches in [2], [3] use the unaliased high venc measurement, \tilde{r}_{21} , to unwrap the low venc measurement, \tilde{r}_{31} , while venc_{32} goes unused. The estimator in [3], which we denote as *standard dual venc* (SDV), is given by

$$\hat{v} = \begin{cases} \tilde{r}_{21} - 4\text{venc}_{31}, & \frac{\tilde{r}_{21} - \tilde{r}_{31}}{2\text{venc}_{31}} \in (-2.4, -1.6) \\ \tilde{r}_{21} - 2\text{venc}_{31}, & \frac{\tilde{r}_{21} - \tilde{r}_{31}}{2\text{venc}_{31}} \in (-1.2, -0.8) \\ \tilde{r}_{21} + 2\text{venc}_{31}, & \frac{\tilde{r}_{21} - \tilde{r}_{31}}{2\text{venc}_{31}} \in (0.8, 1.2) \\ \tilde{r}_{21} + 4\text{venc}_{31}, & \frac{\tilde{r}_{21} - \tilde{r}_{31}}{2\text{venc}_{31}} \in (1.6, 2.4). \end{cases} \quad (26)$$

In [5], two potentially aliased measurements $\tilde{r}_{31}, \tilde{r}_{32}$ are jointly unwrapped by minimizing

$$\hat{v} = \underset{v \in [-\Omega/2, \Omega/2]}{\text{argmin}} 2 - \sum_{l=(31,32)} \cos\left(\frac{\pi v}{\text{venc}_l} - \theta_l\right). \quad (27)$$

The authors dub their approach *optimal dual venc* (ODV), and the minimization is accomplished by searching $v \in$

$[-\Omega/2, \Omega/2)$ with grid spacing $\text{venc}_{31}/1000$. The cost adopted in ODV is equivalent to

$$\frac{1}{2} \sum_{l=31,32} \left\| \exp\left(i \frac{\pi v}{\text{venc}_l}\right) - \exp(i\theta_l) \right\|_2^2. \quad (28)$$

The ODV approach recommends $\text{venc}_{32} = \frac{3}{2}\text{venc}_{31}$, yielding an unaliased range of $[-3\text{venc}_{31}, 3\text{venc}_{31})$. The choice $\frac{3}{2}$ is a heuristic to lessen the probability of unwrapping errors when minimizing (27) in the presence of noise. Finally, the maximum likelihood estimate [10] in additive white Gaussian noise is the least-squares fit of parameters (A, ϕ_0, v) directly to the complex data in (4). This is likewise accomplished by searching a grid of values, $v \in [-\Omega/2, \Omega/2)$, and for each candidate v the best $Ae^{i\phi_0}$ is the average of the L complex-valued points $\tilde{y}_l e^{-im_{1l}v}$, $l = 1, \dots, L$.

E. PRoM

Observe that the velocity estimate, \hat{v} , is a function of the remainders, $\tilde{\mathbf{r}}$, which lie in a hyper-rectangle $[0, 2\text{venc}_{31}) \times [0, 2\text{venc}_{32}) \times [0, 2\text{venc}_{21})$. We introduce a fast estimator based on (13) and detection of the wrapping integers, \mathbf{k} . We refer to (13) and this detector together as *Phase Recovery from Multiple Wrapped Measurements* (PRoM). The algorithm extends the prior signal processing result in [11] to accommodate correlated phase errors and to provide fast computation of the wrapping integers. PRoM provides a grid-free alternative to searching over v for the best least-squares fit in (4) or (27).

Assuming $v \in [0, \Omega]$, define the set \mathcal{K}' of wrapping integers

$$\mathcal{K}' = \{\mathbf{k} \mid -\mathbf{1} \preceq \mathbf{k} \preceq \mathbf{h}\} \quad (29)$$

$$\mathbf{h} = \left[\frac{\Omega}{2\text{venc}_{31}}, \frac{\Omega}{2\text{venc}_{32}}, \frac{\Omega}{2\text{venc}_{21}} \right]^T. \quad (30)$$

By (16), $\mathbb{P}(\mathbf{k} \in \mathcal{K}') \approx 1$. So, from (13) and (17), we can write the reduced likelihood

$$\hat{v} = \arg \min_v \mathcal{L}, \quad v \in [0, \Omega) \quad (31)$$

$$\approx \arg \min_v \mathcal{L}, \quad v \in \{\langle \mathbf{w}^T(\tilde{\mathbf{r}} + 2\mathbf{k} \circ \mathbf{venc}) \rangle_\Omega, \mathbf{k} \in \mathcal{K}'\}, \quad (32)$$

with probability ≈ 1 . Next, we can decrease the cardinality of the search set, \mathcal{K}' , denoted by $|\mathcal{K}'|$. First, because $\mathbf{w}^T \mathbf{1} = 1$ (14), we have

$$\langle \mathbf{w}^T(\tilde{\mathbf{r}} + 2\mathbf{k} \circ \mathbf{venc}) \rangle_\Omega = \langle \mathbf{w}^T(\tilde{\mathbf{r}} + 2(\mathbf{k} + \mathbf{h}) \circ \mathbf{venc}) \rangle_\Omega. \quad (33)$$

From (33), we see that \mathbf{k} and $\mathbf{k} + \mathbf{h}$ generate the same \hat{v} . Second, because $2\mathbf{k} \circ \mathbf{venc} + \tilde{\mathbf{r}} = \mathbf{v} \mathbf{1} + \mathbf{n}$ and invoking (16),

$$\mathbb{P}(\max(\mathbf{k} - \mathbf{1}) \circ 2\mathbf{venc} < \min(\mathbf{k} + \mathbf{1}) \circ 2\mathbf{venc}) \approx 1. \quad (34)$$

Thus, the pruned search set for PRoM can be expressed

$$\mathcal{K} = \{\mathbf{k} \mid -\mathbf{1} \preceq \mathbf{k} \preceq \mathbf{h}, -\mathbf{1} \not\preceq \mathbf{k} - \mathbf{h}, \max(\mathbf{k} - \mathbf{1}) \circ \mathbf{venc} < \min(\mathbf{k} + \mathbf{1}) \circ \mathbf{venc}\}. \quad (35)$$

For example, with $\mathbf{venc} = [10, 14, 35]^T$, we have $|\mathcal{K}'| = 252$ and $|\mathcal{K}| = 39$. An approximate maximum likelihood velocity estimator, PRoM, for L -point encoding is given in Alg. 1. The code is available in <https://github.com/Zhao-Shen/PRoM>.

Algorithm 1 PRoM for L -Point Encoding

Require: Complex noise power, σ^2 ; Gyromagnetic ratio, γ ; First moments, m_{11}, \dots, m_{1N} ; Complex-valued measurements, $\tilde{\mathbf{y}}$.

- 1: Calculate $\mathbf{venc}, \tilde{\mathbf{r}}, \Omega, \mathcal{K}$ via (6, 8, 9, 35)
- 2: Calculate $\text{snr}^2 = \frac{\|\tilde{\mathbf{y}}\|^2}{L\sigma^2}$
- 3: Calculate $\Sigma(\mathbf{n})$ and \mathbf{w} using snr via (11, 23, 14)
- 4: Compute $\hat{v}_{\mathbf{k}}$ for each $\mathbf{k} \in \mathcal{K}$ via (13)
- 5: Select $\hat{v}_{\mathbf{k}^*} = \text{argmin} \mathcal{L}(\tilde{\mathbf{r}}, \hat{v}_{\mathbf{k}})$, $\mathbf{k} \in \mathcal{K}$ via (19)

Ensure: Velocity estimate, $\hat{v}_{\mathbf{k}^*}$

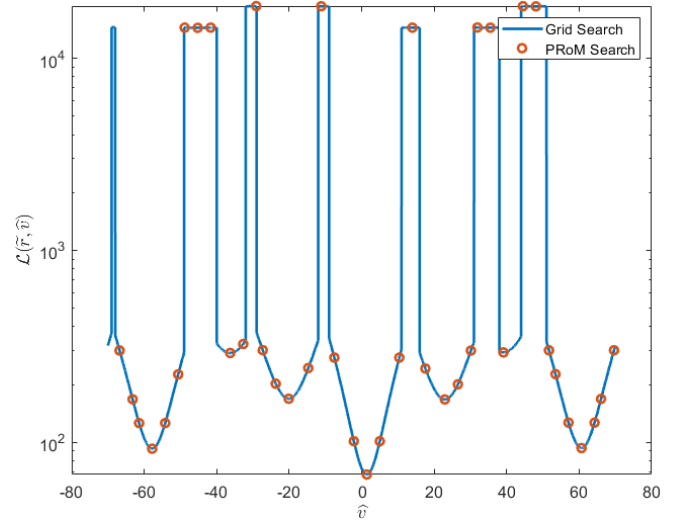


Fig. 2. Cost $\mathcal{L}(\tilde{\mathbf{r}}, \hat{v})$, for $\tilde{\mathbf{r}} = [1, 2, 3]^T$, $\mathbf{venc} = [10, 14, 35]^T$, $\text{snr} = 5$. The red dots mark the PRoM search over candidate wrapping integers in \mathcal{K} .

Fig. 2 illustrates the negative log likelihood, $\mathcal{L}(\hat{v})$, with searched values for $\mathbf{k} \in \mathcal{K}$ marked by superimposed red dots. If the velocity range is known and restricted to be much less than Ω , then the set of search points \mathcal{K} may be further pruned accordingly. And, the endpoints of the reduced range should also be included into the possible \hat{v} candidates.

The PRoM approximate maximum likelihood estimator admits a simple geometric interpretation. Noiseless remainders lie in the hyper-rectangle on the parallel line segments formed by wrapping $v\mathbf{1}$, $v \in [0, \Omega)$. Then, \hat{v} is found by an oblique projection of the noisy remainders to the closest line segment, where “oblique” and “closest” are defined by the weighted distance using $\Sigma^{-1}(\mathbf{n})$. The search for the closest line segment is reduced to searching over wrapping integers in \mathcal{K} . To illustrate the computation complexity, consider the case in Fig. 2: grid search over velocity entails 7000 distance computations [5] and results in a small bias and slightly increased RMSE due to the quantized values of velocity and impractical assumption of independence of correlated noise; search over all wrapping integers in \mathcal{K}' would require 252 distance computations, while PRoM requires search over $|\mathcal{K}| = 39$ possible triples of wrapping integers and returns a grid-free velocity estimate.

F. Conditional Distribution of the Estimate

Knowing the distribution, $\mathbb{P}(\hat{v}|v)$, of the estimate given the true velocity enables optimized design of \mathbf{venc} and the underlying first moments. To derive the distribution, we first establish two lemmas.

Lemma 1: Suppose \mathbf{k}^* minimizes $\mathcal{L}(\tilde{\mathbf{r}}, \hat{v}_{\mathbf{k}})$, then \mathbf{k}^* also minimizes $\mathcal{L}(\tilde{\mathbf{r}}', \hat{v}_{\mathbf{k}})$, where $\tilde{\mathbf{r}}' = \tilde{\mathbf{r}} + c\mathbf{1}$ and $c \in [-\min \mathbf{r}, \min(2\mathbf{venc} - \mathbf{r})]$.

Proof: Since $d_{2\mathbf{venc}}(\tilde{\mathbf{r}}, x) = d_{2\mathbf{venc}}(\tilde{\mathbf{r}}', x + c)$,

$$\operatorname{argmin}_x \mathcal{L}(\tilde{\mathbf{r}}, x) = \operatorname{argmin}_x \mathcal{L}(\tilde{\mathbf{r}}', x) - c.$$

Thus

$$\begin{aligned} \hat{v}(\tilde{\mathbf{r}}') &= \hat{v}(\tilde{\mathbf{r}}) + c \\ &= \mathbf{w}^\top(\tilde{\mathbf{r}} + 2\mathbf{k}^* \circ \mathbf{venc})_{\Omega} + c \\ &= \mathbf{w}^\top(\tilde{\mathbf{r}}' + 2\mathbf{k}^* \circ \mathbf{venc})_{\Omega}. \end{aligned}$$

So, \mathbf{k}^* also minimizes $\mathcal{L}(\tilde{\mathbf{r}}', \hat{v}_{\mathbf{k}})$. ■

Lemma 2:

$$n_i - n_1 \perp \mathbf{w}^\top \mathbf{n}, i \neq 1 \quad (36)$$

Proof:

$$\begin{aligned} \operatorname{cov}(\mathbf{w}^\top \mathbf{n}, n_i - n_1) &= \mathbf{w}^\top \mathbb{E}(\mathbf{n}(n_i - n_1)) \\ &= \frac{\mathbf{1}^\top \Sigma^{-1}(\mathbf{n}) \Sigma(\mathbf{n}) (\mathbf{e}_i - \mathbf{e}_1)}{\mathbf{1}^\top \Sigma(\mathbf{n})^{-1} \mathbf{1}} \\ &= 0, i \neq 1, \end{aligned} \quad (37)$$

where \mathbf{e}_i is standard basis equal to 1 at i -th position and 0 otherwise. ■

Armed with the lemmas, we can specify the distribution.

Theorem 1: Given v , for all noisy remainders $\tilde{\mathbf{r}}$ sharing the same \mathbf{k}^* the linear estimate $\hat{v}_{\mathbf{k}^*}$ (i.e., without wrapping into the unambiguous range) is normally distributed with mean $2\mathbf{k}^* \circ \mathbf{venc} + \mathbf{r}$ and variance $\mathbf{w}^\top \Sigma(\mathbf{n}) \mathbf{w}$.

The proof is a direct result of $\mathbf{e}_i - \mathbf{e}_1 \perp \mathbf{1}, i \neq 1$ and combination of Lemma 1 and Lemma 2.

Let $\mathcal{D}(\hat{v}|\mathbf{k}^*, v)$ denote this conditional probability density function (PDF) without wrapping into the unambiguous range. Then, we can divide the hyper-rectangle of remainders into regions $\mathcal{R}(\mathbf{k}^*)$, each including all $\tilde{\mathbf{r}}$ that share the same wrapping integers \mathbf{k}^* . Fig. 3 provides visualisation of decision regions in the hyper-rectangle for the case $\mathbf{venc} = [10, 14, 35]$, $\operatorname{snr} = 5$. All points along $\mathbf{1}$ direction share the same \mathbf{k}^* , which is proven in Lemma 1.

In Fig. 3, the points shaded with the same color correspond to the same region, $\mathcal{R}(\mathbf{k}^*)$. Define $\mathbb{P}(\mathbf{k}^*|v) = \mathbb{P}(\tilde{\mathbf{r}} \in \mathcal{R}(\mathbf{k}^*)|v)$. Thus, by wrapping the PDF function and invoking the law of total probability, we have

$$\mathbb{P}(\hat{v}|v) = \sum_{\mathbf{k}^* \in \mathcal{K}} \mathbb{P}(\mathbf{k}^*|v) \mathcal{F}(\hat{v}|\mathbf{k}^*, v) \quad (38)$$

$$\mathcal{F}(\hat{v}|\mathbf{k}^*, v) = \begin{cases} \sum_{i \in \mathbb{Z}} \mathcal{D}(\hat{v} + i\Omega|\mathbf{k}^*, v), & \hat{v} \in [0, \Omega) \\ 0, & \text{otherwise} \end{cases} \quad (39)$$

To complete (38), we need only to calculate $\mathbb{P}(\mathbf{k}^*|v)$ by integration of a multivariate normal distribution. Leveraging Lemma 1, the integration can be simplified to a definite integration of a normal distribution in $L - 1$ variables.

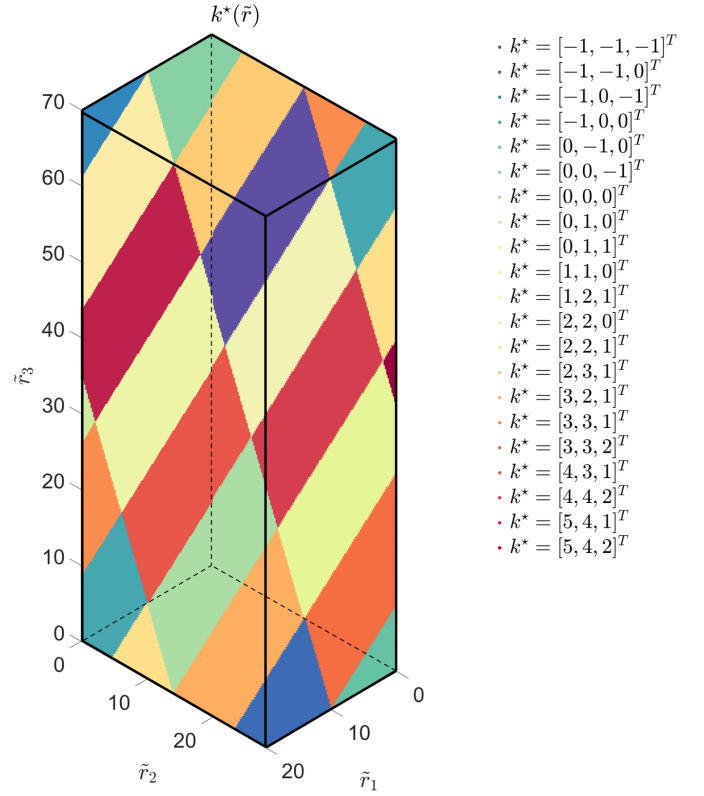


Fig. 3. Example of decision regions for wrapping integers, $\mathbf{venc} = [10, 14, 35]$, $\operatorname{snr} = 5$. The colored tiles for each region are drawn on the surfaces of the hyper-rectangle, and regions extend unchanged parallel to the $[1, 1, 1]^\top$ direction, which is the direction of the line of sight in the figure. PRoM detects wrapping integers for fast, accurate estimation of velocity.

Examples of $\mathbb{P}(\hat{v}|v)$ at $\mathbf{venc} = [18, 22, 99]^\top$ at $\operatorname{snr} = 2$ and $\operatorname{snr} = 5$ are shown in Fig. 4.

G. Design

The selection of the pair \mathbf{venc}_{31} and R defines first moments $[m_{11}, m_{12}, m_{13}]$ up to translation. The choice entails the interplay of noise sensitivity, probability of correct unwrapping, and the range of reliably unaliased velocities. We adopt a performance guarantee strategy for navigating these competing objectives. The design inputs are: the maximum range of velocities to be reliably detected Ω_{rel} , an operating snr , and bounds on the per-pixel probability of an unwrapping error. The design outputs are the \mathbf{venc} and an underlying $[m_{11}, m_{12}, m_{13}]$. To formalize the notion of optimality, we make four definitions.

Definition 1 (Unwrapping error): If $\mathbf{k}^*(\tilde{\mathbf{r}}) \neq \mathbf{k}$, i.e., wrapping integers are incorrectly detected, then we say an *Unwrapping Error* occurs.

Definition 2 (Aliasing error): If $\mathbf{k}^*(\tilde{\mathbf{r}}) = \mathbf{k}$, i.e., wrapping integers are correctly detected, but the $\hat{v}_{\mathbf{k}^*}$ is aliased, then we say an *Aliasing Error* occurs.

Definition 3 (ϵ -Reliable Range): For a given signal to noise ratio, snr , and two small numbers ϵ_1, ϵ_2 , the ϵ -reliable range Ω_{rel} is the range of the velocities for which $\mathbb{P}(\text{Unwrapping Error}) \leq \epsilon_1$ and $\mathbb{P}(\text{Aliasing Error}) \leq \epsilon_2$.

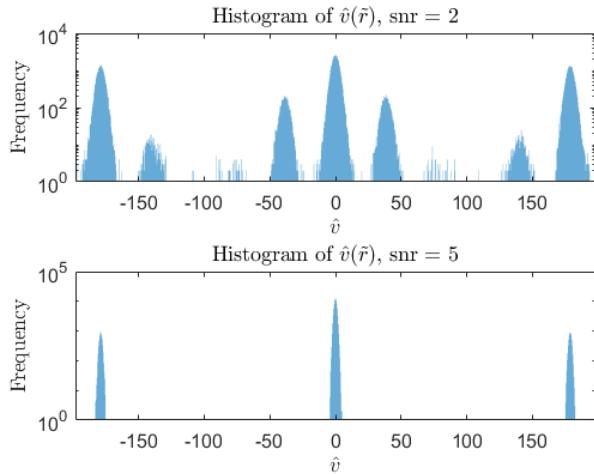


Fig. 4. Histogram of $(\hat{v}|v)$, for $\mathbf{venc} = [18, 22, 99]^T$, $v = 0$, at $\text{snr} = 2$ (top) and $\text{snr} = 5$ (bottom). Number of trials is 10^5 . Note the logarithmic scale for the vertical axis covering four (top) and five (bottom) orders of magnitude. The histogram illustrates both noise sensitivity via the spread of each Gaussian component and the probability of unwrapping errors via the presence of multiple components.

Definition 3 allows us to specify a reliable velocity range that is less than the LCM of $2\mathbf{venc}$ to guard against aliasing. Armed with these three definitions, we can now state a precise meaning of optimality for three-point design.

Definition 4 (Optimal \mathbf{venc} Design): Given the snr for the complex-valued data, the desired maximum velocity range of length Ω_{rel} , and unwrapping error bounds ϵ_1, ϵ_2 , the optimal \mathbf{venc} minimizes the RMSE among all designs for which the unwrapping and aliasing errors satisfy $\mathbb{P}(\text{Unwrapping Error}) \leq \epsilon_1$ and $\mathbb{P}(\text{Aliasing Error}) \leq \epsilon_2$ across the entire range of length Ω_{rel} .

Given snr and \mathbf{venc} , $\mathbb{P}(\text{Unwrapping Error})$ can be calculated through Monte Carlo simulation by setting $v = 0$ and counting the trials for which $\mathbf{k}^* \neq \mathbf{0}$. Symmetry of the decision regions allows simulation of $v = 0$ to be sufficient. The number of trials is selected as $100/\epsilon_1$ [12].

Bounding aliasing error can be achieved via explicitly designing Ω different than Ω_{rel} . Let the normal cumulative distribution function be $\Phi(\cdot)$. Then, $\mathbb{P}(\text{Aliasing Error}) \leq \epsilon_2$ when

$$\Omega - \Omega_{\text{rel}} \geq 2\Phi^{-1}(1 - \epsilon_2)\sqrt{\mathbf{w}^T \boldsymbol{\Sigma}(\mathbf{n}) \mathbf{w}}. \quad (40)$$

In addition, scaling \mathbf{venc} and Ω_{rel} by the same factor does not affect $\mathbb{P}(\text{Unwrapping Error})$ or $\mathbb{P}(\text{Aliasing Error})$, so we can search over rational numbers, $R = p/q \in (1, 2)$, to numerically find the optimal \mathbf{venc} . The searching range \mathcal{R} is

$$\mathcal{R} = \left\{ \frac{p}{q} \mid \gcd(p, q) = 1, \frac{p}{q} \in (1, 2), p \leq P, q \leq Q \right\}, \quad (41)$$

where $\gcd(\cdot, \cdot)$ is greatest common divisor of \cdot , and P, Q are predefined upper bounds on the positive integers p, q . Thus the numerical procedure to optimally design \mathbf{venc} is detailed in Alg. 2.

Algorithm 2 PRoM Optimized Design of \mathbf{venc}

Require: $P, Q, \text{snr}, \Omega_{\text{rel}}, \epsilon_1, \epsilon_2$

```

1:  $\sigma = \infty, p = 2$ 
2: while  $p \leq P$  do
3:    $q = 1$ 
4:   while  $q \leq Q$  do
5:     if  $\gcd(p, q) = 1$  and  $\frac{p}{q} \in (1, 2)$  then
6:       Let  $\mathbf{venc} = [q(p - q), p(p - q), pq]$ .
7:       Calculate  $\tilde{\mathbf{r}}, \mathbf{w}, \Omega, \boldsymbol{\Sigma}(\mathbf{n})$ .
8:       Let  $v = 0$ , generate  $\mathbf{y}$  and  $\tilde{\mathbf{r}}$  with  $100\epsilon_1^{-1}$  trials.
9:       if (Frequency of  $\mathbf{k}^* \neq \mathbf{0}$ )  $< \epsilon_1$  then
10:         $c = \left( \Omega - 2\Phi^{-1}(1 - \epsilon_2)\sqrt{\mathbf{w}^T \boldsymbol{\Sigma}(\mathbf{n}) \mathbf{w}} \right) / \Omega_{\text{rel}}$ 
11:        if  $c\sqrt{\mathbf{w}^T \boldsymbol{\Sigma}(\mathbf{n}) \mathbf{w}} \leq \sigma$  then
12:           $\mathbf{venc} = [cq(p - q), cp(p - q), cpq]$ 
13:           $\sigma = c\sqrt{\mathbf{w}^T \boldsymbol{\Sigma}(\mathbf{n}) \mathbf{w}}$ 
14:        end if
15:      end if
16:    end if
17:     $q \leftarrow q + 1$ 
18:  end while
19:   $p \leftarrow p + 1$ 
20: end while

```

Ensure: \mathbf{venc}

III. METHODS AND RESULTS

A. Simulation

We use numerical simulation to compare both estimation performance and \mathbf{venc} design. Additionally, we explore the approximations in (16) and (17). First, to assess estimation performance we adopt $\mathbf{venc} = [6, 10, 15]^T$ at $\text{snr} = 10$. The ODV estimation algorithm uses $\tilde{\mathbf{r}}_{31}, \tilde{\mathbf{r}}_{32}$, while SDV uses $\tilde{\mathbf{r}}_{31}, \tilde{\mathbf{r}}_{21}$. We calculate RMSE averaged over 10^5 trials at each true v on $[-30, 30]$ sampled every 0.1. The results are shown in Fig. 5.

The velocity range unwrapped by ODV and PRoM can be much larger than the range for SDV by virtue of jointly unwrapping two or more potentially wrapped phase measurements. Both ODV and PRoM show noise-induced aliasing errors when the true velocity is near ± 30 cm/s, whereas the same happens for SDV at ± 15 cm/s. Within the common range that all three methods can reliably unwrap, PRoM has the lowest RMSE. whereas ODV has the highest RMSE.

Next, we compare the design of \mathbf{venc} given $\text{snr} = 10$ and $\Omega_{\text{rel}} = 300$, meaning that the desired velocity range to be estimated is $[-150, 150]$. The SDV and ODV techniques specify the three \mathbf{venc} s to be $\mathbf{venc} = [50, 75, 150]$. For PRoM, the design procedure in Alg. 2 results in $p/q = 7/4$ and $c = 1.83$, yielding $\mathbf{venc} = [21.90, 38.33, 51.10]^T$ via Alg. 2, Step 12. Both Unwrapping Error and Aliasing Error are bounded to be below 10^{-6} in the PRoM design. RMSE results for 1000 trials at each true velocity value with grid 0.1 are shown in Fig. 6. The SDV and ODV approaches share the same acquisition strategy; SDV computation uses (50, 150) whereas ODV jointly unwraps two phase differences from (50, 75) with ratio $R = 3/2$. The PRoM design explicitly suppresses both Unwrapping Errors and Aliasing Errors to

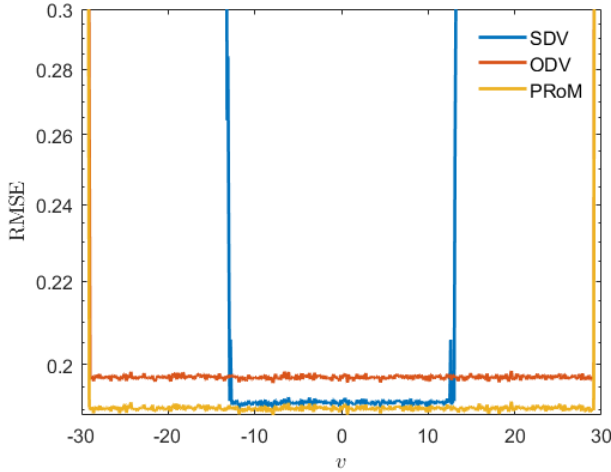


Fig. 5. RMSE versus true v for $\mathbf{venc} = [6, 10, 15]^T$ and $\text{snr} = 10$. RMSE values are averaged over 10^5 trials.

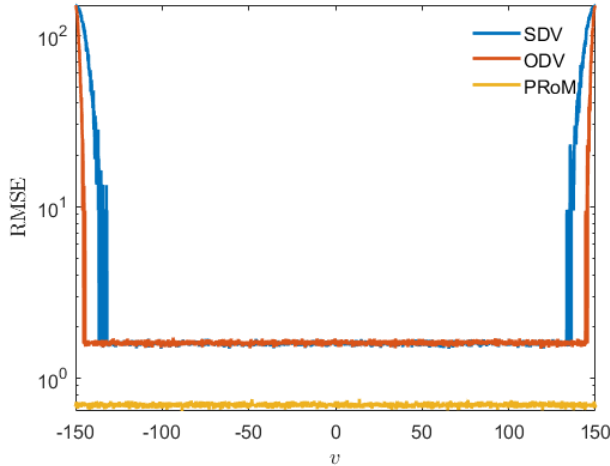


Fig. 6. Comparison of acquisition design and estimation for SDV, ODV, and PRoM: RMSE versus true velocity. Desired velocity range to be estimated is $[-150, 150]$. For SDV and ODV the three \mathbf{venc} generated are $\mathbf{venc} = [50, 75, 150]^T$, whereas PRoM uses $\mathbf{venc} = 1.82[12, 21, 28]^T$. RMSE values are averaged over 10^3 trials.

ensure reliable estimation across the full range, $[-150, 150]$, while also providing smaller RMSE using $R = 7/4$.

PRoM processing depends on the two approximations identified above. First, the noise-induced perturbations on the angle differences, $\hat{\theta}_{ab}$, are assumed to be jointly Gaussian with covariance $\Sigma(\mathbf{n})$. Second, noise is smaller than the modulus in (8). These approximations are numerically explored in Fig. 7 for $\mathbf{venc} = [6, 10, 15]$. The square root of the Cramér-Rao lower bound (CRLB) [9, p. 364] derived from complex measurements is plotted versus snr for the model in (4) with equal amplitudes. The CRLB provides a lower bound on the error variance for any unbiased estimator; the bound is from a local analysis of the likelihood function, and thus optimistically does not consider unwrapping errors. Superimposed are the RMSE values for both MLE and PRoM calculated using 10^5 trials;

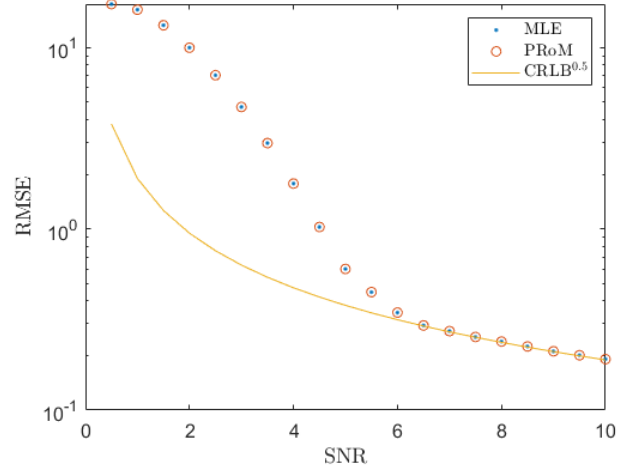


Fig. 7. Comparison of PRoM, the maximum likelihood estimate directly from the complex-valued pixels, and the Cramér-Rao bound. RMSE is graphed versus SNR; RMSE values for MLE and PRoM are averaged from 10^5 trials.

the MLE from the complex measurements uses grid search on v with spacing 0.006. For low snr , both estimators diverge from the bound due to unwrapping errors. For high snr (here, approximately above 5), both the MLE and PRoM achieve the square root of CRLB. Moreover, throughout the range of noise powers, the RMSE difference between MLE and PRoM is negligible, hence justifying the characterization of PRoM as an approximate maximum likelihood estimator.

B. Phantom

A phantom experiment allows for a controlled comparison of competing estimation algorithms. The authors are grateful to Dr. Ning Jin and Siemens Healthineers for facilitating the phantom experiment. An agarose gel-filled cylindrical container is used to generate the MRI signal. An air-coupled propeller rotates the container. The rotational rate is counted with a photomicrosensor [13]. The velocity increases linearly with the distance from the center of the container. In this experiment, we encode the vertical component of the in-plane velocity, which ranges from -240 to 240 cm/s, using a three-point acquisition. Some of the acquisition parameters include: $\mathbf{venc} = [100, \frac{500}{3}, 250]$ cm/s; field-of-view (FOV), 520×260 mm; flip angle, 5° ; TR, 4.38 ms; TE, 2.66 ms; matrix size 192×125 . Results in Fig. 8 illustrate that SDV and PRoM can unwrap more pixels with velocities close to ± 250 cm/s, consistent with the simulated RMSE results in Fig. 5.

C. In Vivo

A healthy volunteer was scanned on a 1.5 T scanner (Siemens MAGNETOM Avanto) with an IRB-approved protocol. A single breath-held PC-MRI dataset was collected, with the imaging plane intersecting both the ascending aorta and descending aorta. Other acquisition parameters include: FOV, 800×250 mm; flip angle, 15° ; TR, 5.99 ms; TE, 3.11 ms; matrix size 120×80 ; cardiac phases, 14. The three-point

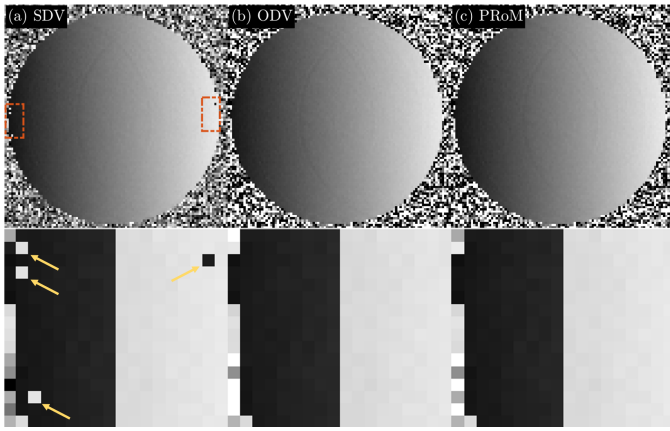


Fig. 8. Comparison of estimators for SDV, ODV, and PRoM. $\mathbf{venc} = [100, \frac{500}{3}, 250]^T$ cm/s. The in-plane speed is in the range $[-240, 240]$ cm/s.

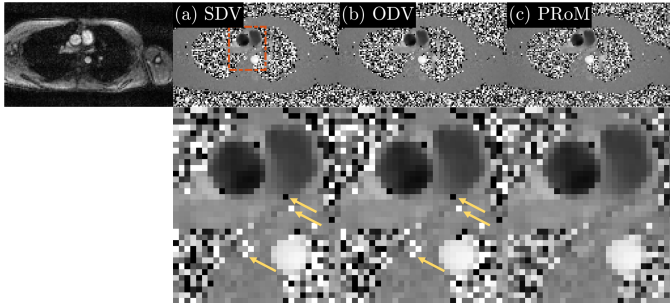


Fig. 9. Comparison for SDV, ODV, and PRoM velocity estimation for $\mathbf{venc} = [40, 60, 120]^T$ cm/s. The top left is the magnitude image corresponding to m_{12} , which has the smallest absolute value of first moment.

acquisition of $\mathbf{venc} = [40, 60, 120]^T$ cm/s per the ODV and SDV design is adopted to allow comparison of estimators on equal footing. The \mathbf{venc} scouting scan shows the velocity is less than 80 cm/s; this information is used in PRoM to reduce \mathcal{K} and to add ± 80 cm/s to the candidate values of \hat{v} .

From Fig. 9, PRoM is seen to unwrap more pixels close to the boundaries of the aorta as well as other pixels in positions with the low signal-to-noise ratio.

IV. DISCUSSION

The proposed PRoM algorithm provides an approximate maximum likelihood estimator for unwrapping multiple noisy phase differences. For solving a system of noisy congruence equations, PRoM extends current signal processing art to accommodate correlated noise and to provide fast detection of wrapping integers. By jointly unwrapping three phase differences, PRoM achieves lower RMSE than standard dual \mathbf{venc} for the same acquisition:

$$\frac{\text{RMSE}_{\text{PRoM}}}{\text{RMSE}_{\text{SDV}}} = \sqrt{\frac{1 + 3\text{snr}^2}{1 + 2\text{snr}^2} \frac{R^2}{2(R^2 - R + 1)}}. \quad (42)$$

For example, at $\text{snr} = 10$ and $R = 11/10$, the free benefit is 9.66% reduction of RMSE given no unwrapping error.

Moreover, the unambiguous range with PRoM may be much larger than the highest \mathbf{venc} (22), as illustrated in Fig. 5. PRoM provides a fast, grid-free solution for velocity, yet the search over the pruned set of candidate wrapping integers is up to two orders of magnitude faster than the grid-search for velocity in traditional nonlinear least-squares estimation. Moreover, for batch processing at a fixed snr , the decision regions $\mathcal{R}(\mathbf{k}^*)$ can be pre-constructed using a small collection of linear boundaries on the faces of the hyper-rectangle, allowing detection of \mathbf{k}^* with approximately $\log_2 |\mathcal{K}|$ complexity.

The PRoM algorithm naturally yields a probability distribution on the estimated velocity, from which the experiment design can be optimized. The design approach presented here minimizes RMSE given guaranteed bounds on probabilities of unwrapping and aliasing errors. Moreover, the design explicitly provides the subset, $[-\Omega_{\text{rel}}/2, \Omega_{\text{rel}}/2]$, of the unambiguous range on which the errors are reliably avoided. The resulting design departs from existing heuristics. The design provides guarantees for a given snr , which may vary voxel to voxel. For any higher snr , the probabilities of Unwrapping Error and Aliasing Error decrease further below the guaranteed level, and the error variance, $\mathbf{w}^T \Sigma(\mathbf{n}) \mathbf{w}$, also decreases. As the target snr used for design increases, Alg. 2 returns higher values of the product pq ; conversely, for $\text{snr} < 5.9$, the value $p/q = 3/2$ is returned, matching the heuristic in [5].

In this paper, we make no assumption regarding referenced or symmetric encoding (other than in Appendix II); \mathbf{venc} depends only on the set of all pairwise differences, $|m_{1a} - m_{1b}|$. As a result, a three-point acquisition with first moments $[m_{11}, m_{12}, m_{13}]$ yields the same \mathbf{venc} when adding a constant to each first moment or when multiplying all by -1 . In both ODV [5] and “triple \mathbf{venc} ” [14] approaches, two angle differences, θ_{31} and θ_{32} , share a common reference, m_{13} , and are called “low- \mathbf{venc} ” and “high- \mathbf{venc} ”, respectively, whereas the third phase difference, θ_{21} , yields the highest \mathbf{venc} (called “intrinsic \mathbf{venc} ” in [14]). Both ODV and triple \mathbf{venc} recover a velocity estimate on the range given by this intrinsic \mathbf{venc} : $(-\mathbf{venc}_{21}, \mathbf{venc}_{21})$. ODV does this by jointly unwrapping measurements θ_{31} and θ_{32} using $R = 3/2$, while triple \mathbf{venc} uses the higher \mathbf{venc} measurements to unwrap the lowest \mathbf{venc} measurement, θ_{31} . In contrast, PRoM can unwrap a velocity range $(p - q)$ larger, where $R = p/q \in (1, 2)$ is the ratio of \mathbf{venc}_{32} to \mathbf{venc}_{31} . Alg. 2 informs us how large $(p - q)$ can be while still reliably unwrapping all three measurements, for a given snr , ϵ_1, ϵ_2 . Further, PRoM faithfully accounts for VNR differences and noise correlations among the three measured phase differences to combine all three into a velocity estimate. ODV uses only θ_{31} and θ_{32} and neglects both the VNR differences and the correlation. Triple \mathbf{venc} uses only the unwrapped θ_{31} to compute a velocity estimate, eschewing the small VNR gain accessible via a properly weighted combination of all three phase differences.

For multi-coil data processing, one could choose to simply apply the PRoM algorithm with N_c times the number of congruence equations, where N_c denotes the number of coils. However, we find that first combining the coils is not only faster but also provides lower RMSE (results not shown). Let y_a^i denote the a^{th} acquisition observed in the i^{th} coil; the

coil combining is given by $\tilde{\theta}_{ab} = \angle \left(\sum_{i=1}^{N_c} \tilde{y}_a^i \tilde{y}_b^{i*} \right)$. Indeed, this is simply the phase from the off-diagonal entries of the “multi-snapshot covariance matrix” typically used in array processing [9, p. 278].

PRoM performs estimation only on a per pixel basis. If additional information is assumed about the local relationships among velocities across time or space, then Bayesian post-processing can enhance unwrapping performance [15]. To this end, (19) provides a confidence measure for each candidate $k \in \mathcal{K}$, which is necessary for fusion of information in the Bayesian context.

APPENDIX I COVARIANCE MODELING

In this appendix, we derive the covariance matrix for the phase differences from L -point encodings with consideration of dephasing. The complex double Gaussian distribution [16] is the joint (amplitude, phase) distribution of the product of two independent non-zero-mean Complex Gaussian random variables. This probability distribution function is a doubly infinite summation over modified Bessel functions of the first and second kinds; the number of terms needed for accuracy is dependent upon the Rician-factors of the two input variables. For the linear unbiased estimator in (13), we require only the mean and variance of the marginal distribution on phase and the covariance of two such angles, which we approximate below.

Recall from (4) that the complex noise samples n_k are independent with variance $\sigma^2/2$ in each of the uncorrelated zero-mean real and imaginary parts. The mean and variance of $\tilde{y}_a \tilde{y}_b^*$ are [16]:

$$\mathbb{E}(\tilde{y}_a \tilde{y}_b^*) = A_a A_b e^{i\gamma(m_{1a} - m_{1b})v} \quad (43)$$

$$\sigma^2(\tilde{y}_a \tilde{y}_b^*) = \sigma^2(A_a^2 + A_b^2) + \sigma^4. \quad (44)$$

From (43)-(44), the squared signal-to-noise ratio (or Rician factor), for the complex-valued random variable $\tilde{y}_a \tilde{y}_b^*$ is,

$$\text{SNR}^2(\tilde{y}_a \tilde{y}_b^*) = \frac{|\mathbb{E}(\tilde{y}_a \tilde{y}_b^*)|^2}{\sigma(\tilde{y}_a \tilde{y}_b^*)^2} = \frac{A_a^2 A_b^2}{\sigma^2(A_a^2 + A_b^2) + \sigma^4} \quad (45)$$

$$= \frac{\text{snr}_a^2 \text{snr}_b^2}{\text{snr}_a^2 + \text{snr}_b^2 + 1}. \quad (46)$$

In (46), we use lowercase snr_a to denote A_a/σ for a complex-valued voxel measurement \tilde{y}_a . When $\text{SNR}(\tilde{y}_a \tilde{y}_b^*)$ is large, the distribution of angle is close to a normal distribution. Note $\sigma(\tilde{\theta}_{ab})$ is inversely proportional to $\text{SNR}(\tilde{y}_a \tilde{y}_b^*)$, since $\lim_{x \rightarrow 0} x/\tan(x) = 1$,

$$\begin{aligned} \sigma^2(\tilde{\theta}_{ab}) &\approx \frac{1}{2 \text{SNR}^2(\tilde{y}_a \tilde{y}_b^*)} \\ &= \frac{1 + \text{snr}_a^2 + \text{snr}_b^2}{2 \text{snr}_a^2 \text{snr}_b^2}. \end{aligned} \quad (47)$$

With similar derivation, for the covariance we have

$$\begin{aligned} \text{cov}(\tilde{\theta}_{ab}, \tilde{\theta}_{cb}) &\approx \frac{|\text{cov}(\tilde{y}_a \tilde{y}_b^*, y_c \tilde{y}_b^*)|}{2A_a A_b^2 A_c} \\ &= \frac{1}{2 \text{snr}_b^2}. \end{aligned} \quad (48)$$

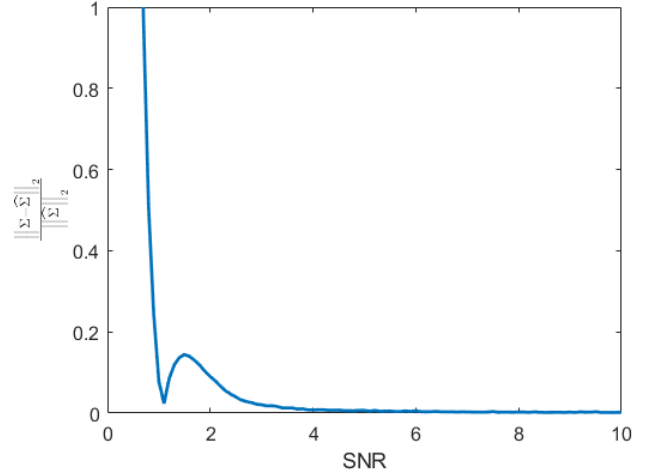


Fig. 10. Covariance matrix modeling error versus SNR, computed using 10^6 trials at each SNR value. The error is the normalized spectral norm of the matrix difference between the derived approximate covariance Σ and experimental covariance $\tilde{\Sigma}$.

Then, for three-point acquisition

$$\text{cov}(\tilde{\theta}) \approx \begin{bmatrix} \frac{1 + \text{snr}_3^2 + \text{snr}_1^2}{2 \text{snr}_3^2 \text{snr}_1^2} & \frac{1}{2 \text{snr}_2^2} & \frac{1}{2 \text{snr}_1^2} \\ \frac{1}{2 \text{snr}_2^2} & \frac{1 + \text{snr}_3^2 + \text{snr}_2^2}{2 \text{snr}_3^2 \text{snr}_2^2} & -\frac{1}{2 \text{snr}_2^2} \\ \frac{1}{2 \text{snr}_1^2} & -\frac{1}{2 \text{snr}_2^2} & \frac{1 + \text{snr}_3^2 + \text{snr}_1^2}{2 \text{snr}_3^2 \text{snr}_1^2} \end{bmatrix}. \quad (49)$$

The corresponding covariance matrix for wrapped velocity measurements, $\tilde{\mathbf{r}}$, is

$$\Sigma(\mathbf{n}) \approx \frac{\text{venc}_{31}^2}{\pi^2} \mathbf{D} \text{cov}(\tilde{\theta}) \mathbf{D}, \quad (50)$$

where $\mathbf{D} = \text{diag} \left(\left[1 \ R \ \frac{R}{R-1} \right] \right)$. As seen in Fig. 10, when $\text{SNR} > 3$ and increases, the approximation error is very small and approaches 0. Thus the approximation is accurate at modest SNR.

To use the general covariance model in velocity estimation, we simply use observed voxel magnitudes to estimate snr_a for each encoding, then calculate \mathbf{w} in (14) and apply PRoM to do the estimation.

APPENDIX II DESIGN WITH BOUND ON FIRST MOMENT

In the presence of dephasing, one may desire to minimize the largest first moment to mitigate the loss of signal strength, because dephasing increases with the magnitude of the first moment [2], [8]. This desire implies a symmetric three-point acquisition, i.e., $m_{11} < m_{12} < 0 < m_{13}, m_{11} = -m_{13}$, and for design we adopt an upper bound, m_c , on the largest first moment. The resulting modification to the optimized design is given in Alg. 3.

To illustrate, an example with first moment constraint is shown in Fig. 11, where $\text{snr} = 10$ and $\Omega_{\text{rel}} = 300$. The SDV and ODV techniques specify the three venc s to be [50, 75, 150] using a referenced encoding, resulting in a largest absolute value of first moment equal to $\frac{\pi}{50\gamma}$. Adopting this first moment

Algorithm 3 PRoM Optimized Design with Largest First Moment Constraint

Require: $P, Q, \text{snr}, \Omega_{\text{rel}}, \epsilon_1, \epsilon_2, m_c$

```

1:  $\sigma = \infty, p = 2$ 
2: while  $p \leq P$  do
3:    $q = 1$ 
4:   while  $q \leq Q$  do
5:     if  $\text{gcd}(p, q) = 1$  and  $\frac{p}{q} \in (1, 2)$  then
6:       Let  $\mathbf{venc} = [q(p-q), p(p-q), pq]$ 
7:       Calculate  $\tilde{\mathbf{r}}, \mathbf{w}, \Omega, \Sigma(\mathbf{n})$ .
8:       Let  $v = 0$ , generate  $\mathbf{y}$  and  $\tilde{\mathbf{r}}$  with  $100\epsilon_1^{-1}$  trials.
9:       if (Frequency of  $\mathbf{k}^* \neq \mathbf{0}$ )  $< \epsilon_1$  then
10:         $c = (\Omega - 2\Phi^{-1}(1 - \epsilon_2)\sqrt{\mathbf{w}^\top \Sigma(\mathbf{n}) \mathbf{w}}) / \Omega_{\text{rel}}$ 
11:         $c = \max\left(c, \frac{\pi}{2\gamma m_c q(p-q)}\right)$ 
12:        if  $c\sqrt{\mathbf{w}^\top \Sigma(\mathbf{n}) \mathbf{w}} \leq \sigma$  then
13:           $\mathbf{venc} = [cq(p-q), cp(p-q), cpq]$ 
14:           $\sigma = c\sqrt{\mathbf{w}^\top \Sigma(\mathbf{n}) \mathbf{w}}$ 
15:        end if
16:      end if
17:    end if
18:     $q \leftarrow q + 1$ 
19:  end while
20:   $p \leftarrow p + 1$ 
21: end while
22:  $m_{11} = -m_{13} = \frac{\pi}{-2\gamma \text{venc}_{31}}$ 
23:  $m_{12} = \frac{\pi}{2\gamma \text{venc}_{31}} - \frac{\pi}{\gamma \text{venc}_{32}}$ 
Ensure:  $[m_{11}, m_{12}, m_{13}]$ 

```

as an upper bound, PRoM in Alg. 3 results in a symmetric encoding with largest first moment of $\frac{\pi}{51.21\gamma}$, $\frac{p}{q} = \frac{6}{5}$ and $\mathbf{venc} = 5.12[5, 6, 30]^\top$. As in the unconstrained case in Section III.A, PRoM results in both lower RMSE and wider reliable range, as seen in Fig. 6.

Finally, we recall that the set of acquired \mathbf{venc} s remains unchanged if a constant is added to each of the three first moments; thus, if a referenced encoding is desired, then the set of first moments may be translated to place $m_{12} = 0$, leaving $m_{11} < 0$ and $m_{13} > 0$. The resulting venc_{21} and venc_{32} would then be encodings both referenced to a zero first moment, with venc_{31} providing a third (or ‘‘intrinsic’’ [14]) velocity encoding.

REFERENCES

- [1] N. J. Pelc, R. J. Herfkens, A. Shimakawa, D. R. Enzmann *et al.*, ‘‘Phase contrast cine magnetic resonance imaging,’’ *Mag. Reson. Quarterly*, vol. 7, no. 4, pp. 229–254, 1991.
- [2] A. T. Lee, G. B. Pike, and N. Pelc, ‘‘Three-point phase-contrast velocity measurements with increased velocity-to-noise ratio,’’ *Magn. Reson. Med.*, vol. 33, pp. 122–126, 1995.
- [3] S. Schnell *et al.*, ‘‘Accelerated dual- venc 4D flow MRI for neurovascular applications,’’ *J. Magn. Reson. Imaging*, vol. 46, no. 1, pp. 102–114, 2017.
- [4] S. Zhao, L. C. Potter, N. Jin, Y. Liu, O. P. Simonetti, and R. Ahmad, ‘‘PC-MRI with phase recovery from multiple wrapped measurements (PRoM),’’ in *Proc. 26th ISMRM Meeting & Exhibition*, Paris, France, 2018, p. 0685.
- [5] H. Carrillo, A. Osses, S. Uribe, and C. Bertoglio, ‘‘Optimal dual- venc unwrapping in phase-contrast MRI,’’ *IEEE Trans. Med. Imag.*, vol. 38, no. 5, pp. 1263–1270, 2019.

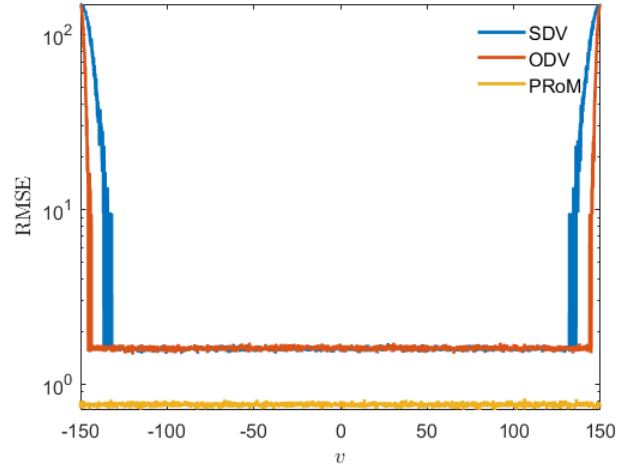


Fig. 11. Comparison for acquisition design and estimation of SDV, ODV, and PRoM: RMSE versus true velocity. Desired velocity range to be estimated is $[-150, 150]$. For SDV and ODV the three \mathbf{venc} s generated are $\mathbf{venc} = [50, 75, 150]^\top$, whereas PRoM uses $\mathbf{venc} = 5.12[5, 6, 30]^\top$. RMSE values are averaged from 10^3 trials.

- [6] W. Wang, X. Li, W. Wang, and X.-G. Xia, ‘‘Maximum likelihood estimation based robust Chinese remainder theorem for real numbers and its fast algorithm,’’ *IEEE Trans. Signal Process.*, vol. 63, no. 13, pp. 3317–3331, 2015.
- [7] M. Wang and A. Nehorai, ‘‘Coarrays, MUSIC, and the Cramér–Rao bound,’’ *IEEE Trans. Signal Process.*, vol. 65, no. 4, pp. 933–946, 2017.
- [8] M. Markl, ‘‘Velocity encoding and flow imaging,’’ in *ISMRM 14th Scientific Meeting & Exhibition*, May 2006.
- [9] P. Stoica and R. Moses, *Spectral Analysis of Signals*. Upper Saddle River, NJ: Prentice-Hall, 2005.
- [10] C. G. Khatri, ‘‘Some results for the singular normal multivariate regression models,’’ *Sankhyā: The Indian Journal of Statistics, Series A*, vol. 30, no. 3, pp. 267–280, 1968. [Online]. Available: <http://www.jstor.org/stable/25041358>
- [11] W. Wang, X. Li, W. Wang, and X.-G. Xia, ‘‘Maximum likelihood estimation based robust Chinese remainder theorem for real numbers and its fast algorithm,’’ *IEEE Trans. Signal Process.*, vol. 63, no. 13, pp. 3317–3331, 2015.
- [12] M. Jeruchim, ‘‘Techniques for estimating the bit error rate in the simulation of digital communication systems,’’ *IEEE J. Sel. Areas Commun.*, vol. 2, no. 1, pp. 153–170, 1984.
- [13] A. Vali, S. Schmitter, L. Ma, S. Flassbeck, S. Schmidt, M. Markl, and S. Schnell, ‘‘Development of a rotation phantom for phase contrast MRI sequence validation and quality control,’’ *Magn. Reson. Med.*, vol. 84, no. 6, pp. 3333–3341, 2020.
- [14] L. E. Ma, M. Markl, K. Chow, A. Vali, C. Wu, and S. Schnell, ‘‘Efficient triple- venc phase-contrast mri for improved velocity dynamic range,’’ *Magn. Reson. Med.*, vol. 83, no. 2, pp. 505–520, 2020.
- [15] A. Rich, L. C. Potter, N. Jin, J. Ash, O. P. Simonetti, and R. Ahmad, ‘‘A Bayesian model for highly accelerated phase-contrast MRI,’’ *Magn. Reson. Med.*, vol. 76, no. 2, pp. 689–701, 2016.
- [16] N. O’Donoghue and J. M. Moura, ‘‘On the product of independent complex Gaussians,’’ *IEEE Trans. Signal Process.*, vol. 60, no. 3, pp. 1050–1063, 2012.